Propane Dehydrogenation Using Platinum Supported on Gallium-Doped Silica

Xin Li[1] · Peng Rui[1] · Wenfei Huang[1] · Xin Yao[1] · Yuewen Ye[1] · Tongqi Ye[1] · David J. Morgan[2,3] · James H. Carter[2]

Abstract

The dehydrogenation of propane over Pt supported on Ga- doped silica was investigated, using various meso- and microporous silica supports. The addition of a small amount of Ga (0.5 wt%) to SBA-15 was enough to boost the resultant 1 wt% Pt catalyst's conversion from < 5 up to 38%. Propene selectivity also increased from around 60 to 98%. Optimisation of the Pt and Ga content revealed that low loadings of both active components are necessary to increase the efficiency of the reaction and beyond this only modest improvements in performance were obtained. A range of pore structures were investigated, but the Ga content was found to be more important than the support morphology; without sufficient Ga incorporation into the support the catalyst could not achieve high conversion and selectivity. Post-reaction analysis suggested that coke formation blocking sites was the most likely explanation for catalyst deactivation. These results show that doping Ga into SiO_2 as a support for Pt nanoparticles is a viable strategy for producing highly efficient catalysts for propane dehydrogenation.

Graphical Abstract

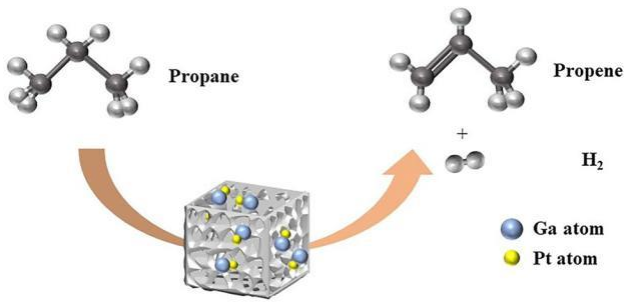

Keywords Propane dehydrogenation · Platinum · Gallium · Propene

✉\ Tongqi Ye
\ yetq@hfut.edu.cn

✉\ James H. Carter
\ carterj5@cardiff.ac.uk

[1]\ Anhui Province Key Laboratory of Advanced Catalytic Materials and Reaction Engineering, School of Chemistry and Chemical Engineering, Hefei University of Technology, Hefei, Anhui, People's Republic of China

[2]\ Max Planck-Cardiff Centre on the Fundamentals of Heterogeneous Catalysis FUNCAT, Cardiff Catalysis Institute, School of Chemistry, Cardiff University, Cardiff CF10 3AT, UK

[3]\ Harwell XPS, Research Complex at Harwell (RCaH), Didcot OX11 0FA, UK

1 Introduction

Propene is a bulk chemical and important precursor to poly-propene, acetone, acetonitrile and others. Traditionally, propene was produced exclusively by indirect petrochemical processes including catalytic cracking of naphtha and syngas/methanol-mediated routes [1]. While these methods still constitute the majority of propene production, the direct or on-purpose dehydrogenation of propane to propene has become an established alternative, with many advantages over indirect production. Firstly, in the direct dehydrogenation reaction the atomic economy is much higher (than in cracking), there are no toxic reagents and there are

opportunities to use renewable feedstocks [1]. Additionally, H_2 is produced as a valuable by-product.

There are various commercialised processes for propane dehydrogenation, including Oleflex, STAR, Dow FCDh process, CATOFIN and K-PRO [1]. With the exception of the final process (where the catalyst has not been disclosed), either Pt or Cr are utilised as the active component of the catalyst. The catalysts are vulnerable to deactivation by coking, shown by the very short cycle times used, which can be 1–15 min [2]. Catalyst regeneration is carried out by burning the coke off in a regeneration cycle, which increases the carbon footprint of the process as well as limiting propene yields. This also necessitates complex reactor design, with several parallel beds rotating through dehydrogenation, purging and regeneration stages [2].

Many non-precious metal catalysts have been investigated for PDH. Notable examples include vanadium, chromium, gallium, zinc oxide and cobalt oxide [2–6]. Ga has been extensively studied, and is typically supported on -SiO_2 or Al_2O_3. In these catalysts, maximum dispersion of oxidised Ga is essential for high activity, and any loss of dispersion is detrimental for performance [7–9]. However, these mixed metal oxide catalysts are intrinsically less active than precious metals [1].

Pt is by far the most-studied precious metal for PDH, but like most PDH catalysts, without modification/promotion, is unstable and catalyses deep dehydrogenation to coke [10, 11]. Therefore the development of a coke-resistant catalyst for this reaction is highly desirable, hence the continuing interest in academia and industry in this research field. Among the major breakthroughs in PDH catalysis is the discovery that the addition of Ga (or Sn) to Pt can dramatically improve the performance. In the case of Sn, the promotion is observed as an enhancement in propene selectivity [1]. The beneficial effect of combining Pt and Ga was originally reported by Jablonski et al., who added Ga as a promotor to supported Pt catalysts [12]. Since then, numerous studies have emerged that have further elucidated the synergy observed in Pt–Ga catalysts [13]. Recently, Zhang et al. investigated the mechanism of Pt–GaO_x synergy when using Ga_2O_3 as a support [14]. It was shown that the Pt promoted H_2 dissociation and surface coverage of H species, which aided C_3H_8 activation. Pt–Ga alloy formation was observed at higher loadings of Pt, which inhibited H species formation and overall C-3 H_6 formation. On the other hand, Pt–Ga alloy formation has been reported to be necessary for inhibiting coke formation [2].

Although PtGa-catalyzed propane dehydrogenation supported by -Al_2O_3 and -SiO_2 have been reported, we noticed that the influence of SiO-2 structure on performance of PtGa catalyst hasn't been covered. As we all know, -SiO_2 can form a variety of structures, such as amorphous SiO-2 and mesoporous molecular sieves SBA-15, MCM-48, etc. Therefore, here we prepared different gallium-containing SiO_2 supports to clarify the influence of SiO-2 architecture on PtGa catalysts in this work. Additionally, it is generally believed that Pt reduces Ga- $_2O_3$ through hydrogen overflow to form PtGa alloy active centers. However, few people discuss the role of Ga itself on Pt. Therefore, the effect of the presence of Ga on the charge transfer of surface Pt atoms was investigated by DFT (Density functional theory) calculations.

2 Experimental

2.1 Materials

Hydrochloric acid (HCl) was purchased from Sinopharm Chemical Reagent Co., Ltd. Tetraethyl orthosilicate (TEOS), Gallium nitrate hydrate ($Ga(NO_3)_3{\cdot}xH_2O$), Tetrapropylammonium hydroxide solution (TPAOH, 25% in water), Sodium hydroxide (NaOH), Silicon dioxide (SiO-2, 20 nm), n-Butanol (BuOH), Chloroplatinic acid hexahydrate ($H_2PtCl_6{\cdot}6H_2O$) were purchased from Shanghai Macklin Biochemical Co., Ltd. Pluronic P123 (EO20 -PO70-EO20) was purchased from Sigmaaldrich company. All the chemicals were of analytical grade.

2.2 Catalyst Preparation

The catalyst supports such as the series Ga-SBA-15 were synthesized following the acid-free route reported previously [15]. In a typical preparation of Ga-SBA-15, Pluronic P123 was dissolved in 120 mL of deionized water and stirred for 4 h at the atmosphere temperature. Then, gallium nitrate was added into the solution and the mixture was further stirred for 0.5 h. Afterwards, TEOS was added into the clear solution and vigorously stirred for 15 h at room temperature. The obtained mixture was kept at 40 °C for 24 h under stirring, then transferred into an autoclave and heated at 90 °C for 2 days. The obtained solid precipitate was recovered by filtration, washed several times with deionized water, and dried at 60 °C overnight. It was then calcined at 550 °C for 6 h. The final gallium-doped SBA-15 sample was named x-Ga-SBA-15 (where x = the wt% of Ga, ie. 1.15, 0.58, 3.45 or 5.75). The synthesis methods of Ga-MFI, Ga-MCM-48 and Ga-KIT-6 were the same with previous reports [16–18]. The final molar composition of Ga-MFI and Ga-MCM-48 were 1 TEOS: 0.32 TPAOH: 45.4 -H $_2$O: 0.02 Ga and 1 TEOS: 0.26 NaOH: 0.595 CTMABr: 72 H-2O: 0.02 Ga. Ga-KIT- 6 was synthesized under acidic conditions. The theoretical ratios of all the catalysts were synthesized according to the molar ratio of Ga/Si.

Ga-SiO_2 was prepared by impregnation method. Gallium nitrate was loaded on silica and the resulting sample was

dried at 80 °C overnight and then calcined at 550 °C for 6 h. The final gallium-doped SiO_2 sample was named x-Ga-SiO_2, as per the nomenclature used above.yPt/xGa- SBA-15, yPt/ xGa-MFI, yPt/xGa-MCM-48, yPt/xGa-KIT-6, yPt/xGa-SiO_2 and yPt/SBA-15 catalysts were prepared by wet impregnation method. Typically, 1.0 g of support was mixed with the appropriate volume of $H_2PtCl_6 \cdot 6H_2O$ aqueous solution (4.5g L^{-1}). The resulting sample was dried at 80 °C over-night (y represent the wt% of Pt).

2.3 Catalyst Characterization

Powder X-ray diffraction (XRD) patterns were recorded on a PANalytical X-pert Pro MPD with a Cu Kα radiation (λ = 0.154 nm). The measurement conditions were in the range of 0.5° < 2θ < 5°, the step length is 0.01° and the dwell time is 30 s per step.

X-ray photoelectron spectroscopy was carried out on a Kratos AXIS ULTRA^{DLD} photoelectron spectrometer utilizing monochromatic Al Kα radiation operating at 144 W (12 mA × 12 kV) power. High resolution and survey scans were performed at pass energies of 40 and 160 eV, respectively, with step-sizes of 0.1 and 1 eV, respectively. A magnetically confined low energy electron charge compensation system was used to minimize sample charging and the resulting spectra were calibrated using adventitious carbon, in the C1*s* region, at 284.8 eV. Spectra were fitted using CasaXPS v2.3.24 [19].

The texture properties including specific surface area, pore size distribution and pore volume were determined by nitrogen adsorption at liquid nitrogen temperature 77 K, using a Micromeritics ASAP 2460 instrument.

The Ga and Pt loadings of the prepared catalysts were determined by ICP-OES using an Agilent 5110. The solid sample was treated with a concentrated mixture of HNO_3/ HF/$HClO_4$ and heated to 230 °C with an electric hot plate until the solution evaporated dry to dissolve all the metals in the catalyst and then diluted with distilled water for analysis.

Transmission electron microscopy (TEM) images of catalysts were captured at 200 kV using a JEM -2100F. The powder sample was ultrasonicated in ethanol, and a small amount of the resulting suspension was deposited on carbon-coated copper grids.

2.4 Catalytic Testing

Direct dehydrogenation of propane was tested in a fixed bed quartz tube reactor with an external diameter of 10 mm and an inner diameter of 7 mm. Reaction temperatures were monitored by internal thermocouple placed in the centre of the catalyst bed. The product was analyzed by gas chromatography with a flame ionization detector (FID) and a TCD detector. The column carrier gas of FID is constant pressure nitrogen (3.5 psi, 0.61 mL/min column flow, measured at 70 °C) and the column carrier gas of TCD is constant pressure hydrogen (20.3 psi, measured at 50 °C). Prior to the reaction, the catalyst was first treated with 20 vol% H_2/N_2 gas mixture (100 mL/min) at 600 °C for 1 h. Then cool down to 580 °C for the reaction. The weight of samples was fixed at 0.1 g. The reaction gas composition is 5.55 mL/min $-C_3H_8$ and 9.45 mL/min $-N_2$. The equilibrium conversion of $-C_3H_8$ was calculated to be 53% under these conditions.

$$C_3H_8 \text{ Conversion (\%)} = \frac{\text{moles of propane (in)} - \text{moles of propane (out)}}{\text{moles of propane (in)}} \times 100\%$$

$$C_3H_6 \text{ Selectivity (\%)} = \frac{\text{moles of propane converted to propylene}}{\text{moles of propane (in)} - \text{moles of propane (out)}} \times 100\%$$

2.5 Density Functional Theory (DFT) Calculations

CP2K code was used for the all DFT calculations [20]. We used the PBE GGA exchange–correlation functional with DFT- D3 dispersion correction to more accurately describe weak interactions [21]. A DZVP-MOLOPT-SR-GTH basis set and a plane-wave cut off of 520 Ry were used [22].

The SiO_2 of β-cristobalite (101) structure was selected to simulate the SBA-15. Besides, one Si atom near the surface was substituted by a Ga atom to simulate the Ga-SBA-15. The models were optimized with the five atomic layers relaxed while the remaining underlying atoms were fixed. The lattice constants of SBA-15 used in our simulation were 14.27 Å × 11.41 Å × 26.87 Å.

3 Results and Discussion

3.1 Ga-Doped SiO_2 Supports

To understand the effect of support porosity, a series of Ga-doped SiO_2 supports were prepared and characterised. Pt was then deposited on these supports via impregnation to form a set of supported catalysts.

To investigate the effect of Ga addition on the formation of the porous supports, XRD was carried out on the samples. Wide-angle XRD was completed for the Pt-containing $-SiO_2$ and MFI samples. The Ga- containing SBA-15, and the Pt and Ga- containing SBA-15 samples were also analysed by XRD to check for Pt or Ga reflections that would indicate the undesirable formation of larger crystallites (Fig. S1a, b). In all cases, there were no reflections due to Ga or Pt in the XRD patterns, which rules out the formation large Pt

\

nanoparticles and crystallite gallium oxide. In the case of SBA-15, MCM-48 and KIT-6, the mesoporous structure can be directly probed using low-angle XRD. The diffractograms are presented in Fig. 1b (the corresponding Ga-free diffractograms shown in Fig. S1c).

Figure 1a shows that the 1Pt/1Ga-SiO_2 sample was amorphous, while the 1Pt/1Ga-MFI exhibited complex XRD reflections. The principal reflections were at 7.98°, 8.82°, 23.18° and 24.46°, corresponding to (101), (020), (151) and (303) of silicalite-1 [23]. In Fig. 1b the typical reflections at 0.9° and 2.2° for SBA-15, KIT-6 and MCM-48 were observed, indicative of the spacing of mesopores through-out the samples, confirming that the addition of Ga did not destroy the pore structure. Specifically, the (100), (110) and (200) reflections of SBA-15 were observed at 0.95°, 1.61° and 1.90°. The broad reflection at 2.25° in MCM-48 is due to the (211) reflection. In the case of KIT-6, the reflection at 0.95° due to the (211) lattice plane is rather broad, which indicates that the sample is nanocrystalline. Additionally, Fig. S1 shows the Ga-free KIT-6 sample, which exhibited a (332) reflection at 2.04°, indicating that the introduction of Ga decreased the crystallinity of the sample. KIT- 6 and MCM- 48 without Ga addition exhibited a shift in the position of the reflection to a higher 2θ angle. This indicates a contraction in lattice spacing associated with the mesopore, which may indicate a smaller mesopore.

The specific surface area and pore structure of the catalysts was also investigated to ensure that the values were in agreement with those reported for these supports. The results of the different SiO_2 supports are shown in Table 1, and additional samples and adsorption isotherms in Table S1 and Figs. S2a–c. The specific surface area values are in agreement with those reported for KIT- 6, MFI, MCM-48 and SBA-15 [23–25]. The corresponding adsorption isotherms in Fig. S2a show various isotherm shapes. The SBA-15, MFI,

Table 1 BET results for various SiO_2 supports with Ga incorporation

Catalysts	S_{BET} (m^2/g)	V_p (cm^3/g)	D_p (nm)
1Pt/1Ga-KIT-6	640	0.19	4.1
1Pt/1Ga-MFI	460	0.12	6.1
1Pt/1Ga-SiO_2	140	0.64	24.5
1Pt/1Ga-MCM-48	770	0.51	3.1
1Pt/1Ga-SBA-15	730	0.55	5.6

SiO_2 , and MCM-48 all exhibit isotherm shapes consistent with previous reports, which indicates along with the XRD and BET data that the incorporation of Ga and impregnation of Pt did not compromise the porous structures [24, 25]. However, in the case of KIT-6, the hysteresis loop is much smaller than typically observed, indicating that the total pore volume may be reduced [25].

Table 2 shows the nominal and measured loading of Pt and Ga in the samples, as determined by ICP-OES. The measured Pt loading is generally in good agreement with the theoretical amount, falling within 10% of the target value. Exceptions to this were 1Pt/1Ga-MCM-48, 0.5Pt/1Ga-SBA-15 and 1.5 Pt/1Ga- SBA-15 where the values were closer to 80% of the target loading. The Ga content was also measured, and it was found that a significant proportion of the Ga was not detected in the final product. Theoretical values of 1.15 wt% were typically used, but the actual loadings were closer to 0.49 wt%. The MFI and -SiO_2 supports showed 0.97 and 0.89 wt% Ga, while the KIT-6 sample had only 0.06 wt% Ga present. In the case of KIT-6, this sample also exhibited a smaller than expected pore volume, as discussed above. Overall this sample did not retain the intended physical and chemical properties. The ICP-OES data suggests that the precipitation of Ga under the conditions used to prepare the SiO_2 supports was not efficient, or Ga was lost during the

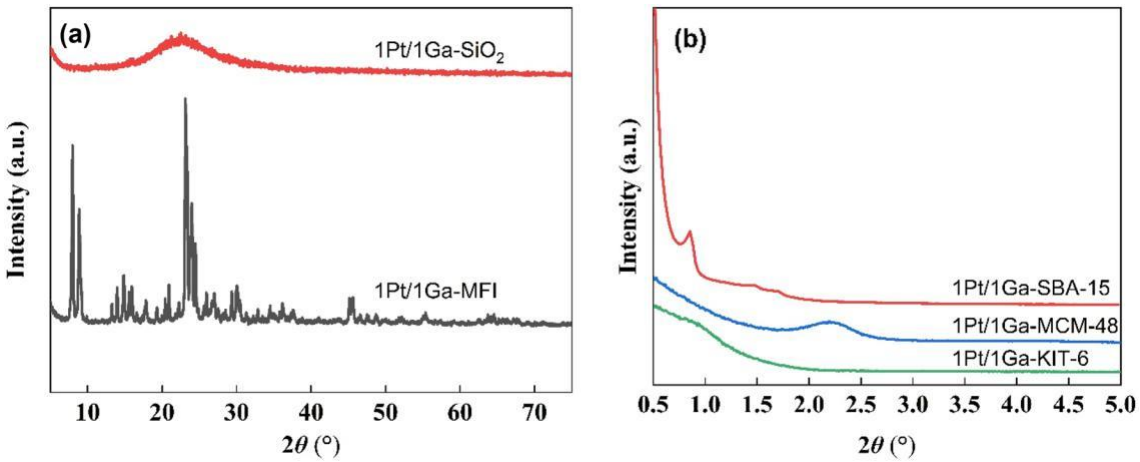

Fig. 1 **a** Wide angle and **b** low angle XRD patterns of fresh catalysts

Table 2 ICP-OES results of the prepared Pt/Ga-silica catalysts

Catalyst	Pt (wt%)		Ga (wt%)	
	Theoretical	Measured	Theoretical	Measured
1Ga-SBA-15	0.00	0.00	1.15	0.51
1Pt/SBA-15	1.00	0.91	0.00	0.00
1Pt/1Ga-MFI	1.00	1.07	1.15	0.97
1Pt/1Ga-SiO_2	1.00	1.03	1.15	0.89
1Pt/1Ga-MCM-48	1.00	0.89	1.15	0.55
1Pt/1Ga-SBA-15	1.00	0.93	1.15	0.49
1Pt/1Ga-KIT-6	1.00	1.01	1.15	0.06
0.2Pt/1Ga-SBA-15	0.20	0.18	1.15	0.49
0.5Pt/1Ga-SBA-15	0.50	0.38	1.15	0.48
1.5Pt/1Ga-SBA-15	1.50	1.31	1.15	0.49
2Pt/1Ga-SBA-15	2.00	1.93	1.15	0.49
1Pt/0.5Ga-SBA-15	1.00	0.95	0.58	0.24
1Pt/3Ga-SBA-15	1.00	0.92	3.45	1.27
1Pt/5Ga-SBA-15	1.00	0.96	5.75	1.59

washing step. However, overall the preparation was successful in incorporating Ga into the support, although the location of the Ga was not confirmed using the above techniques.

XPS analysis of the fresh catalysts (Table 3) shows the surface composition of the samples. The loading of Ga varies significantly depending on the support, indicating a variability in the efficiency of Ga deposition/precipitation, consistent with the ICP-OES data. It should also be noted that due to the highly porous nature of some of the supports, it is possible that a proportion of the Ga (and Pt) was not detected. In the case of 1Pt/1Ga -KIT-6 and 1Pt/1Ga-MFI, the Ga concentration was 0 and 0.03%. The acidic conditions in the preparation may be explain why gallium nitrate did not precipitate. In contrast, 1Pt/1Ga-SBA-15, 1Pt/1Ga-MCM-48 and 1Pt/1Ga-SiO_2 had Ga concentrations of 0.11, 0.16 and 0.31% respectively. Due to the low loading of Pt on the catalyst (< 0.05 at% Pt), robust deconvolution of the 4f region was not possible.

Table 3 XPS analysis of catalysts

Sample	at%					
	O	C	Si	Ga	Pt	Cl
SBA-15	64.1	5.9	30.0	0	0	0
1Ga-SBA-15	65.8	3.8	30.2	0.14	0	0.05
1Pt/SBA-15	65.8	4.0	30.1	0	0.05	0.09
1Pt/1Ga-SBA-15	66	3.9	29.8	0.11	0.04	0.13
1Pt/1Ga-MCM-48	67.6	3.0	29.1	0.16	0.05	0.19
1Pt/1Ga-MFI	62.0	7.3	30.1	0.03	0.22	0.38
1Pt/1Ga-KIT-6	67.7	2.3	29.9	0	0.05	0.1
1Pt/1Ga-SiO_2	65.1	2.4	32.0	0.31	0.05	0.22

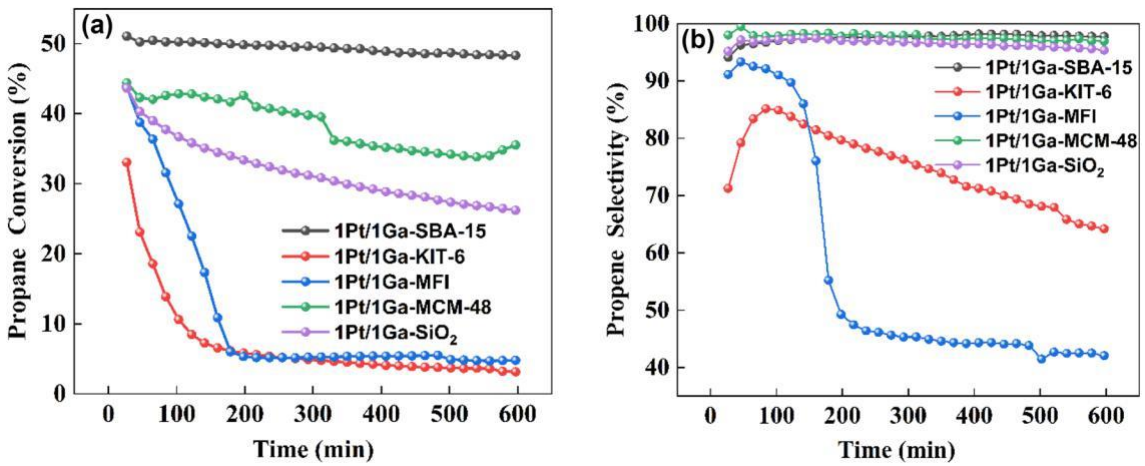

Fig. 2 **a** Conversion of propane and **b** selectivity to propene over a series of different Pt/Ga-doped silica supports

\

3.2 Propane Dehydrogenation Reactions

The influence of the support on the resultant PDH activity was probed by comparing the set of 1 wt% Pt catalysts with various pore architectures. Figure 2a, b shows the reaction data over 600 min on-stream. The performance of the catalyst depends heavily on the support. SBA-15 produced the most active Pt–Ga catalyst (ca. 50% conversion after 600 min on-stream) while KIT-6 and MFI produced the poorest catalysts. The selectivity to propene was also dependent on the support: Pt–Ga supported on -SiO_2, MCM-48 and SBA-15 all exhibited propene selectivity of 95% + whereas in KIT-6 and MFI, the values were 70% and 40% respectively after 600 min on-stream. In the case of the Pt/Ga-MFI catalyst, the initial activity and selectivity were in-line with the Pt/Ga-MCM-48 and Pt/Ga-SiO_2 catalysts. The obvious explanation for the low on-stream stability of the Pt/Ga-MFI catalyst is that the microporous structure of the support means that pore clocking is facile when coke formation occurs, and this in turn rapidly makes the active sites inaccessible. Regarding stability, all the catalysts deactivated on- stream and although the Pt–Ga catalyst appeared stable, the conversion was very close to equilibrium (~ 53%). As a result, the reaction was repeated with half the catalyst mass (Fig. S3). The conversion begins around 27% and decreases to 20% after 30 h on-stream, and the -C_3H_6 selectivity was around 98% throughout the reaction. This represents the most stable catalyst of the series tested and reflects the very low rate of coke formation.

In order to further understand the importance of Ga and Pt content in the catalyst, the loadings were varied systematically over the SBA-15 based catalysts. Figure 3a shows that the catalyst with a nominal loading of Ga at 0.49 wt% gave the best performance. The observed conversion for all the samples was 2, 34, 35, 29 and 24% for the catalysts with 0, 0.24, 0.49, 1.27 and 1.59 wt% Ga, respectively. It is also clear from Fig. 3a that very small loadings of Ga are sufficient to increase the conversion by a large amount, i.e. from ca. 5–48%. A large increase in selectivity towards -C_3H_6 was also observed on the addition of Ga. Above 0.49 wt% Ga, the C_3H_8 conversion decreased and the selectivity remained unchanged (all values were 98%). It has been suggested that Pt–Ga alloy formation can inhibit catalytic activity, and it is possible that at increased Ga concentrations, this occurs [14]. Additionally, the loss of Ga dispersion is a potential explanation of why the conversion drops. Overall, the addition of Ga both increases the number of active sites for PDH, but also minimises deleterious side-reactions such as deep dehydrogenation to coke.

The Pt loading was varied on the 0.49 wt% Ga-SBA-15 support. It was found that the conversion and selectivity were rather insensitive to Pt loading: The conversions were 2, 24, 34, 35, 38 and 37% for the catalysts with 0, 0.18, 0.38, 0.93, 1.31 and 1.93 wt% Pt, respectively. Without Pt, the Ga-SBA-15 catalyst achieved 58% selectivity to C-$3H_6$. Upon the addition of 0.18 wt% Pt, the conversion increased to 24% and the selectivity to above 97%. Further Pt addition resulted in small increases to the conversion (38% conversion at 1.31 wt% Pt) and almost no effect on C-$3H_6$ selectivity (all selectivity measurements were 97–98%). The diminished returns of higher Pt addition might be because there are no available Ga sites to form the highly active sites. In other words, to increase the activity of the catalyst further, both the Ga and the Pt loading must be increased. The molar Ga/Pt ratio in the optimised catalyst was approximately 1.4, which is in contrast to the report of Siddiqi et al. who prepared Ga-doped hydrotalcite supports for Pt nanoparticles [27]. In their work, the optimal ratio was ca. 5.4 and was ascribed to the dilution of Pt by Ga. This suggests a different interaction between Pt and Ga in the current work, as the Ga is part of

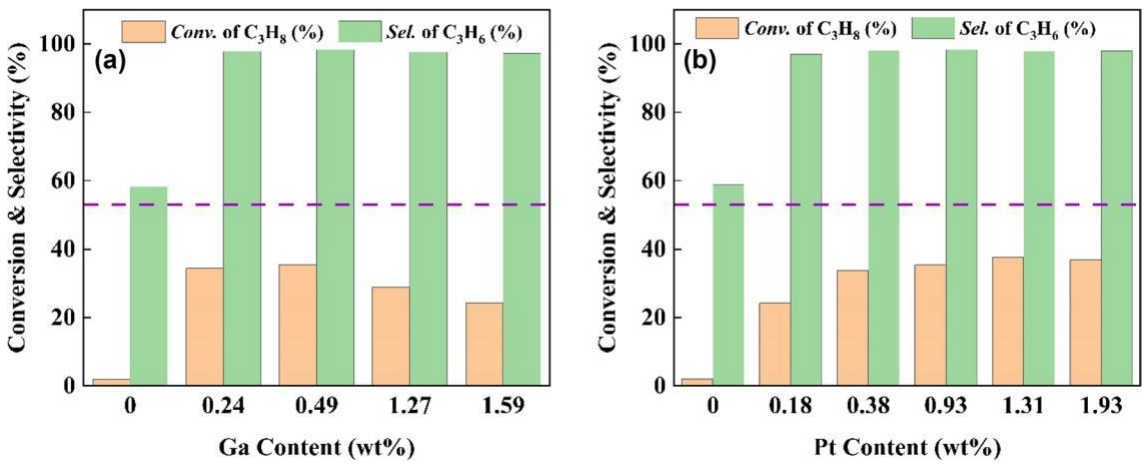

Fig. 3 Influence of **a** Ga and **b** Pt content on the catalytic performance of Pt/Ga-SBA-5 catalysts after 5 h on-stream. The dashed line indicates the equilibrium conversion (reaction conditions: 30 mg catalyst, 580 °C, C-$3H_8/N_2$ = 37:63 (volume), total inlet flow = 15 ml/min)

the support (although may migrate to the Pt surface) and also present in only slight excess. Accordingly, the dilution of Pt by Ga is not expected to be responsible for the high activity observed in the current work. These data, together with those in Fig. 3a highlight the importance of including both Pt and Ga in appropriate quantity, and illustrate the high activity may be achieved without high loadings of precious metal or Ga.

3.3 Role of Ga on Catalyst Stability

The time on-line activity of the most active catalyst, 1Pt/1Ga-SBA-15 was compared to that in the absence of Ga, 1Pt/SBA-15 to understand the impact of Ga on catalyst stability. Fig. S4 shows that 1Pt/SBA-15 deactivates rapidly on-stream and shows only 4.5% conversion after 600 min on-stream. In contrast, the 1Pt/1Ga-SBA-15 catalyst was able to maintain the majority of its activity over the course of the 600 min reaction. It was found that Ga enhances the stability of the catalyst, which is likely related to the decreased formation of coke. It is also possible that the Pt particle size is affected by the presence of Ga, as suggested by Payard et al. [28]. Accordingly, TEM was carried out. Figure 4 shows representative images of Pt/SBA-15 and Pt/Ga-SBA- 15, while additional images of the fresh and used samples are shown in Figs. S5–S7. Although not enough Pt particles were imaged to sustain a statistically robust particle size distribution, it is still possible to infer information on the Pt particles and overall morphology of the catalysts. Fig. S5a, c, e, g show the fresh 1Pt/SBA-15 catalyst. Pt particles 10–20 nm in diameter were observed, as well as smaller particles 5 nm or less in diameter. Interestingly, these were not distributed evenly across the support, and appeared to be in the same small region of the support. This may be due to the evaporation of the solvent during the catalyst preparation leading to inhomogeneous drying of the surface. The used sample also exhibited Pt particles of a similar size, suggesting that Pt particle growth was not the dominant deactivation mechanism. The corresponding TEM analysis of 1Pt/1Ga-SBA-15 is shown in Fig. S6. Similar to 1Pt/SBA-15, the particles of Pt were not distributed equally across the support, but located densely in a small region of sample. Overall the Pt particles appeared to be < 10 nm, although this couldn't be verified statistically. In the used sample, the Pt particles also appeared largely unchanged, also suggesting that Pt particle growth was not a limiting factor in catalyst stability. In all cases, the morphology of the supports remained intact, with the SBA-15 mesopores remaining visible throughout. Due to the highly crystalline nature of the SBA-15 support, finding an area of sample that was sufficiently thin to clearly resolve small (sub-2 nm) Pt particles was quite challenging. 1Pt/Ga-SiO_2 was also examined by TEM to understand the

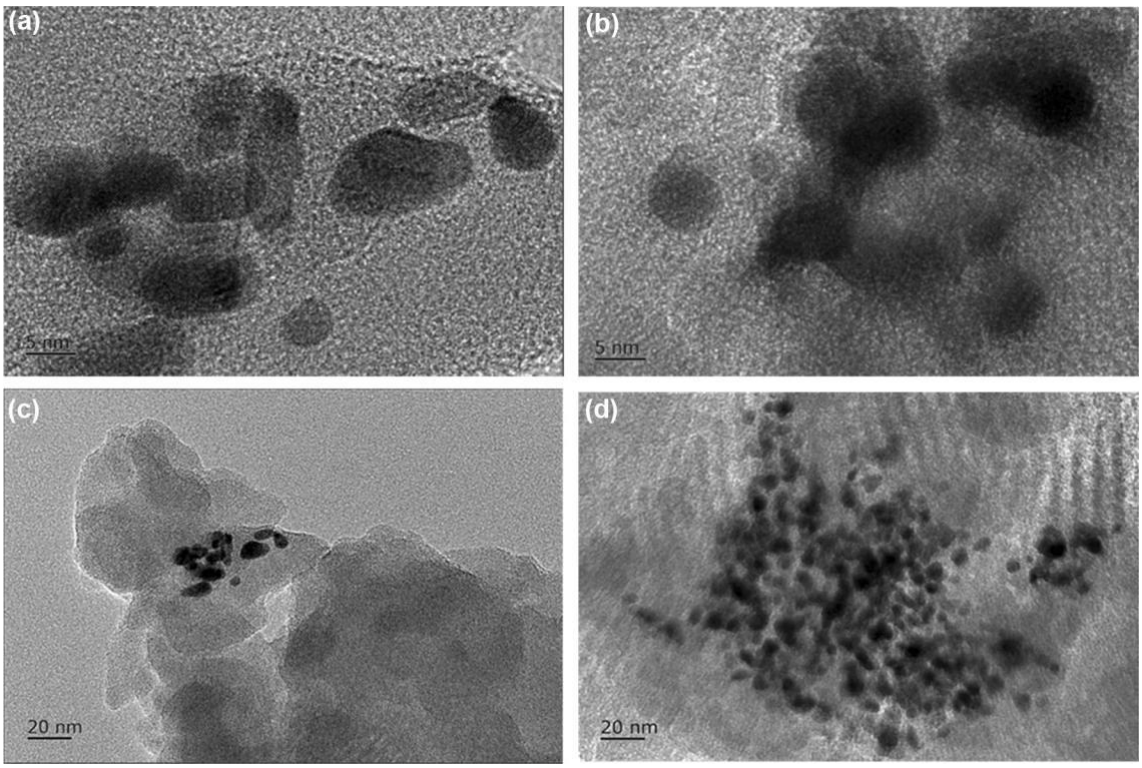

Fig. 4 TEM images of the fresh Pt/SBA-15 (**a**, **c**) and Pt/Ga-SBA-15 (**b**, **d**)

\

structure of a catalyst without an extensive pore network (Fig. S7a–h). As an amorphous support, the crystallite sizes were sub-nanoscopic and the identifying Pt particles was less challenging. In this sample, which was less active and stable than the 1Pt/1Ga-SBA-15 catalyst, the Pt particles were also in the range of 5–15 nm in diameter but were more evenly spread across the entire support surface. Post-reaction analysis showed the presence of similar Pt particles. Without a statistical analysis of the samples, particle growth as a deactivation mechanism can't be ruled out, but it can be concluded that some Pt particles < 5 nm in diameter were stable during the reaction.

XPS analysis of the fresh and used samples was carried out to understand if major changes in the electronic state of the surface could be detected, and if significant carbon deposition had occurred. Table S2 shows the elemental composition of the surface. In both cases, increased carbon on the surface was measured, while differences in Pt or Ga could not be measured. Although the final carbon content of the 1Pt/1Ga-SBA-15 was higher than 1Pt/SBA-15, it should be noted that the Ga-containing catalyst was around 10 × more active than 1Pt/SBA-15, so carbon formation appears quite prevalent. Qualitatively, the more selective catalysts were also more stable on- stream. Coupled with the absence of clear evidence that Pt particles grew during the reaction, it is likely that the main deactivation mechanism was the loss of active sites through site-blocking, i.e. from coke formation.

Assessing the overall performance of the catalysts in the context of the literature is challenging due to the variety of reaction conditions used. However, it is instructive to compare the current results with known PDH catalysts. Table S3 compares the most active catalyst, 1Pt/1Ga-SBA-15, with similar catalysts from the literature. The STY of the major-ity of the literature catalysts are < 95 -mol$_{C3H6}$kg$_{cat}^{-1}$ h^{-1}, whereas the 1Pt/1Ga-SBA-15 catalyst exhibited a value of 170 mol-$_{C3H6}$kg$_{cat}^{-1}$h^{-1}. This demonstrates that the cur-rent approach to preparing highly active PDH catalysts is efficacious.

3.4 DFT Calculations

To further investigate the influence of Ga-doping on the Pt/SiO$_2$ catalyst, DFT was used to calculate electron charge density difference for Pt and Pt–Ga on the SiO-2 surface respectively. The results are shown in Fig. 5, the charge accumulation is denoted in cyan, and charge depletion is in yellow. Focusing on the configuration of Pt on the SiO-2 surface, the electron depletion region mainly locates on the two sides of Pt atom near O atoms from SiO-2, while the electro accumulation region is mostly near O atoms, which shows an obvious electron transfer from Pt to O atoms. In regard to the Pt/Ga-SiO$_2$ surface, the electron depletion region is

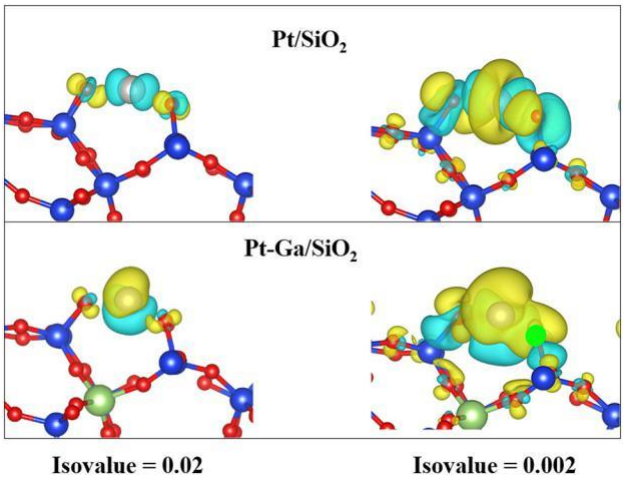

Fig. 5 Isosurface plot of the electron charge density difference for Pt on the SiO-2 surface and Pt–Ga on the SiO-2 surface with the isovalue of 0.02 a.u. (left) and 0.002 a.u. (right) respectively

primarily below Pt atom and region upright above Pt refers to electron accumulation. The above results indicate that the existence of Ga reduces the tendency of electron transfer from Pt to O atoms, therefore Pt is more likely to exist at low valence, which is broadly consistent with literature reports on the role of Ga in modifying the electronic state of Pt [1].

The DFT calculations demonstrate that the co-existence of Pt and framework Ga can produce a chemically distinct active site with modified electronic density. Our TEM analysis revealed that the catalyst consisted of Pt nanoparticles with a broad particle size range, rather than atomically-dispersed Pt species (although we would not expect to be able to resolve these). It is possible that a Pt nanoparticle could also be modified by the existence of Ga at the inter-face of the support-nanoparticle and that this explains the observed enhancement in activity. Alternatively, the Ga may be mobile under reaction conditions and migrate from the support onto the Pt nanoparticle or the interface, via the surface or even via gas-phase transport [12].

4 Conclusions

In conclusion, we have shown that a range of SiO-2 supports can be modified with 0.5 wt% Ga and Pt supported on them to form highly active and selective PDH catalysts. The effect of porosity was probed by selecting a range of pore structures, while the Pt and Ga loadings were optimised. The pore structure was not an important factor in determining the catalyst performance; the level of Ga incorporation was the biggest factor in this. Above 1 wt% Pt, the activity of the catalysts did not improve, while an optimal Ga loading was identified when the Pt loading was 1 wt%. The role

of Ga was further examined by comparing catalysts with and without Ga. There was no evidence that Ga affected the Pt dispersion or stability, and the electronic state of the Pt could not be examined in detail due to the low metal loading. DFT calculations indicated that the presence of framework Ga could reduce the valence of Pt, consistent with previous reports on the effect of Ga addition to Pt catalysts. Our results show that Ga can be doped into different porous SiO_2 supports and serve as an active support in forming highly active Pt–Ga based PDH catalysts.

Acknowledgements The project was supported by Hefei Municipal Natural Science Foundation (2021043) and the Fundamental Research Funds for the Central Universities (JZ2017HGTB0231). XPS data col-lection was performed at the EPSRC National Facility for XPS (‘HarwellXPS’), operated by Cardiff University and UCL, under contract No. PR16195.

Declarations

Conflict of interest The authors have not disclosed any conflict of interest.

References

\ 1.\ Carter JH, Bere T, Pitchers JR, Hewes DG, Vandegehuchte BD, Kiely CJ, Taylor SH, Hutchings GJ (2021) Green Chem 23:9747– 9799. https://doi.org/10.1039/d1gc03700e
\ 2.\ Jeon N, Choe H, Jeong B, Yun Y (2020) Catal Today 352:337–344. https://doi.org/10.1016/j.cattod.2019.12.012
\ 3.\ Meriaudeau P, Naccache C (1989) J Mol Catal 50:L7. https://doi.org/10.1016/0304-5102(89)80103-8
\ 4.\ Liu J, Liu Y, Ni Y, Liu H, Zhu W, Liu Z (2020) Catal Sci Technol 10:1739–1746. https://doi.org/10.1039/c9cy01921a
\ 5.\ Zhao Y, Sohn H, Hu B, Niklas J, Poluektov OG, Tian J, Delferro M, Hock AS (2018) ACS Omega 3:11117–11127. https://doi.org/10.1021/acsomega.8b00862
\ 6.\ Sattler JJHB, Ruiz-Martinez J, Santillan-Jimenez E, Weckhuysen BM (2014) Chem Rev 114:10613–10653. https://doi.org/10.1021/ cr5002436
\ 7.\ Shao CT, Lang WZ, Yan X, Guo YJ (2017) RSC Adv 7:4710–4723. https://doi.org/10.1039/c6ra27204e
\ 8.\ Castro-Fernández P, Mance D, Liu C, Moroz IB, Abdala PM, Pidko EA, Copéret C, Fedorov A, Müller CR (2021) ACS Catal 11:907–924. https://doi.org/10.1021/acscatal.0c05009
\ 9.\ Ni L, Khare R, Bermejo-Deval R, Zhao R, Tao L, Liu Y, Lercher JA (2022) J Am Chem Soc 144:12347–12356. https://doi.org/10.1021/jacs.2c03810
\10.\ Liu G, Zeng L, Zhao ZJ, Tian H, Wu T, Gong J (2016) ACS Catal 6:2158–2162. https://doi.org/10.1021/acscatal.5b02878
11\.\ Nawaz Z, Wei F (2013) Ind Eng Chem Res 52:346–352. https://doi.org/10.1021/ie301422n
12\.\ Jablonski EL, Castro AA, Scelza OA, de Miguel SR (1999) Appl Catal A Gen 183:189–198. https://doi.org/10.1016/S0926-860X(99)00058-7
13\.\ Sun P, Siddiqi G, Chi M, Bell AT (2010) J Catal 274:192–199. https://doi.org/10.1016/j.jcat.2010.06.017
\14.\ Zhang T, Pei C, Sun G, Chen S, Zhao Z, Sun S, Lu Z, Xu Y, Gong J (2022) Angew Chem 61:e202201453. https://doi.org/10.1002/ anie.202201453
\15.\ Cai W, Ni X, Meng F, Sun L, Wang R, Lin S (2022) Microporous Mesoporous Mater 335:11823. https://doi.org/10.1016/j.micro meso.2022.111823
\16.\ Kim W-G, So J, Choi S-W, Liu Y, Dixit RS, Sievers C, Sholl DS, Nair S, Jones CW (2017) Chem Mater 29:7213–7222. https://doi. org/10.1021/acs.chemmater.7b01566
\17.\ dos Santos TG, Silva AOS, Pedrosa AMG, Araujo AS, Souza MJB (2021) J Porous Mater 28:919–928. https://doi.org/10.1007/ s10934-021-01044-w
\18.\ Zhang R, Li T, Zhang Y, Ha J, Xiao Y, Li C, Zhang X, Luo H (2022) Sep Purif Technol:300:121702. https://doi.org/10.1016/j.seppur.2022.121702
\19.\ Fairley N, Fernandez V, Richard-Plouet M, Guillot-Deudon C, Walton J, Smith E, Flahaut D, Greiner M, Biesinger M, Tougaard S, Morgan D, Baltrusaitis J (2021) Appl Surf Sci Adv 5:100112. https://doi.org/10.1016/j.apsadv.2021.100112
\20.\ VandeVondele J, Krack M, Mohamed F, Parrinello M, Chassaing T, Hutter J (2005) Comput Phys Commun 167:103–128. https:// doi.org/10.1016/j.cpc.2004.12.014
\21.\ Becke AD (1988) Phys Rev A 38:3098. https://doi.org/10.1103/PhysRevA.38.3098
22\.\ Becke AD (1993) J Chem Phys 98:5648–5652. https://doi.org/10. 1063/1.464913
\23.\ Malhis AA, Arar SH, Fayyad MK, Hodali HA (2018) Adsorpt Sci Technol 36:270–286. https://doi.org/10.1177/0263617416689270
\24.\ Ghaffari A, Tehrani SM, Husain SW, Aniba M, Azar PA (2014) J Nanostruct Chem 3:114. https://doi.org/10.1007/s40097-014-0114-1
25\.\ Calin N, Galarneau A, Cacciaguerra T, Denoyel R, Fajula F (2010) C R Chim 13:199–206. https://doi.org/10.1016/j.crci.2009.04.001
\26.\ Yang X, Chen J, Lai H, Hu J, Fang M, Luo X (2017) RSC Adv 7:38519–38525. https://doi.org/10.1039/c7ra05863b
\27.\ Siddiqi G, Sun P, Galvita V, Bell AT (2010) J Catal 274:200–206. https://doi.org/10.1016/j.jcat.2010.06.016
28\.\ Payard P-A, Rochlitz L, Searles K, Foppa L, Leuthold B, Safonova O, Comas-Vives A, Copéret C (2021) JACS Au 1:1445–1458. https://doi.org/10.1021/jacsau.1c00212